

# Dynamical conductance in the two-channel Kondo regime of a double dot system

A. I. Tóth,<sup>1,2</sup> L. Borda,<sup>1</sup> J. von Delft,<sup>3</sup> and G. Zaránd<sup>1</sup>

<sup>1</sup>Theoretical Physics Department, Institute of Physics, Budapest University of Technology and Economics, H-1521 Budapest, Hungary

<sup>2</sup>Institute for Theoretische Festkörper Physik, Universität Karlsruhe, D-76128 Karlsruhe, Germany

<sup>3</sup>Physics Department, Arnold Sommerfeld Center for Theoretical Physics and Center for Nanoscience, Ludwig-Maximilians-Universität, D-80333 Munich, Germany

(Received 15 June 2007; published 23 October 2007)

We study finite-frequency transport properties of the double dot system recently constructed to observe the two-channel Kondo effect [R. M. Potok *et al.*, Nature **446**, 167 (2007)]. We derive an analytical expression for the frequency-dependent linear conductance of this device in the Kondo regime. We show how the features characteristic of the two-channel Kondo quantum critical point emerge in this quantity, which we compute using the results of conformal field theory as well as numerical renormalization group methods. We determine the universal crossover functions describing non-Fermi-liquid vs Fermi-liquid crossovers and also investigate the effects of a finite magnetic field.

DOI: [10.1103/PhysRevB.76.155318](https://doi.org/10.1103/PhysRevB.76.155318)

PACS number(s): 72.15.Qm, 73.21.La, 73.23.Hk

## I. INTRODUCTION

In the past few years, semiconducting quantum dots have been in the focus of intense research. This research has mostly been motivated by their possible application in future microelectronics: these devices behave as tunable artificial atoms attached to electrodes.<sup>1</sup> They can be used as single electron transistors.<sup>2</sup> Furthermore, they also serve as a playground to model and study (artificial) molecular transport in a very controlled way. They display a number of correlation-induced effects like the Coulomb blockade or the Kondo effect,<sup>3,4</sup> and they can also give rise to exotic strongly correlated states.<sup>5</sup> Very importantly, quantum dots can also be used to build quantum bits, with the electron spin providing the necessary degree of freedom for quantum computation.<sup>6</sup>

Nevertheless, maybe the most fascinating application of quantum dots is their possible use to realize quantum phase transitions between different correlated states. Several such transitions have been proposed: under special circumstances, the transition between the triplet and the singlet state of a dot can be a true quantum phase transition,<sup>7,8</sup> although in most cases this transition becomes just a crossover.<sup>9</sup> Dissipation<sup>10</sup> can also lead to a quantum phase transition, where the charge degrees of freedom of the dot become localized.<sup>11,12</sup> Unfortunately, these phase transitions have a Kosterlitz-Thouless structure and are, in a sense, “trivial” quantum phase transitions. Using multidot systems, however, it is also possible to realize *generic* quantum phase transitions, where the transition point represents a true critical state characterized by anomalous dimensions and a singular behavior. These critical states are generic non-Fermi-liquid states in the sense that they cannot be described in terms of conduction electron quasiparticles even at the Fermi energy.<sup>13</sup> The prototypes of these generic quantum impurity states are the two-channel Kondo model<sup>14</sup> and the two-impurity Kondo model.<sup>15</sup> Some years ago, Matveev proposed that the two-channel Kondo model could be realized by charge fluctuations at the charge-degeneracy point of a quantum dot.<sup>16</sup> However, Matveev’s mapping assumes a vanishing level spacing, and with present-day technology, it has been impossible to reach this

state so far. However, a few years ago, Oreg and Goldhaber-Gordon proposed to realize the two-channel Kondo state through a double dot system,<sup>17</sup> and after several years of work, this two-channel Kondo state has indeed been observed in a pioneering double dot experiment at Stanford.<sup>18</sup> For the realization of the other prototypical non-Fermi-liquid state, the two-impurity Kondo state, a somewhat similar multidot setup has been proposed recently.<sup>19</sup>

Figure 1 shows the double dot device suggested by Oreg and Goldhaber-Gordon, which has since been used to experimentally reach the two-channel Kondo fixed point.<sup>18</sup> This setup consists of a small dot coupled to a large dot (2) and two leads (1L and 1R). The small dot is tuned to the regime where charge fluctuations are suppressed, and it has only one extra electron on it. The level spacing,  $\delta\epsilon_s$ , of the small dot and its charging energy  $\sim E_{Cs}$  are assumed to be much larger than the temperature,  $\delta\epsilon_s, E_{Cs} \gg T$ , so that below the scale  $D$  charge fluctuations on the small dot are suppressed and the only role of this dot is to provide a spin. The size of the large

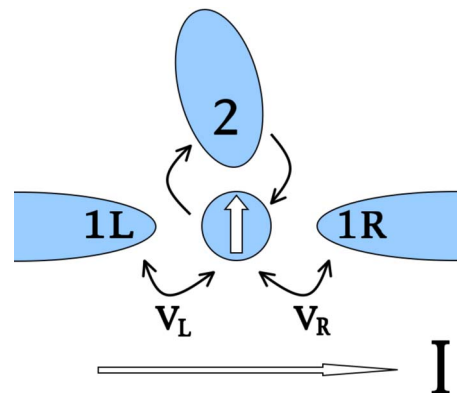


FIG. 1. (Color online) Two-dot device: the small dot in the center couples to a large dot (2) and to a left and a right lead (1L and 1R) via the hopping amplitudes  $v_L$  and  $v_R$ . The small dot has a large level spacing, and the large dot is characterized by a vanishing level spacing, while both dots are in the Coulomb blockade regime. As a result, only spin exchange is possible between the dots.

dot, on the other hand, is chosen in such a way that its charging energy and level spacing satisfy  $E_{C2} > T > \delta\epsilon_2$ . This implies that this dot is also in the Coulomb blockade regime, while the electronic states on it form a continuum of electron-hole excitations. Therefore, electrons on the large dot form a bath that can exchange spin with the small dot, while electrons cannot jump out of it<sup>17</sup> as is also indicated in Fig. 1. In the limit of small tunneling amplitudes, apart from some irrelevant and potential scattering terms, this double dot system is described by the following simple two-channel Kondo Hamiltonian:

$$H_{int} = \frac{1}{2}J_1\vec{S}\psi_1^\dagger\vec{\sigma}\psi_1 + \frac{1}{2}J_2\vec{S}\psi_2^\dagger\vec{\sigma}\psi_2. \quad (1)$$

The operator  $\psi_2$  describes electrons on the large dot. In the continuum limit,  $\delta\epsilon_2 \rightarrow 0$ , it is defined as

$$\psi_{2,\sigma} = \int a_\sigma(\epsilon)d\epsilon, \quad (2)$$

with  $a_\sigma(\epsilon)$  the annihilation operator of a conduction electron of energy  $\epsilon$  and spin  $\sigma$  on the large dot, satisfying the anti-commutation relation  $\{a_\sigma(\epsilon), a_{\sigma'}^\dagger(\epsilon')\} = \delta_{\sigma\sigma'}\delta(\epsilon - \epsilon')$ . The operator  $\psi_1$  in Eq. (1) is a suitably chosen linear combination of electrons on the left and right lead electrodes,

$$\psi_1 = \frac{v_L\psi_L + v_R\psi_R}{(v_L^2 + v_R^2)^{1/2}}, \quad (3)$$

with  $v_L$  and  $v_R$  the hopping amplitudes between the dot and the left and right electrodes, respectively. The left and right fields  $\psi_{L/R}$  are defined similarly to Eq. (2),

$$\psi_{L/R,\sigma} = \int c_{L/R,\sigma}(\epsilon)d\epsilon, \quad (4)$$

with  $c_{L/R,\sigma}(\epsilon)$  the annihilation operator of a conduction electron of energy  $\epsilon$  and spin  $\sigma$  on the left/right lead.

We remark that, strictly speaking, the Kondo Hamiltonian above is only accurate in the limit of small tunneling, while in the experiments, the tunneling rates were quite large in order to boost up the Kondo temperature.<sup>18</sup> Therefore, to study the region far above  $T_K$ , an Anderson-model-type approach would be needed that also accounts for charge fluctuations of the small dot.<sup>20</sup> Nevertheless, our Kondo-model-based approach captures accurately the universal crossover functions in the region of interest, i.e., around and far below the Kondo temperature, provided that both dots are close to the middle of the Coulomb blockade regime. To account for deviations from the middle of the Coulomb blockade valley, one could break the particle-hole symmetry of Eq. (1) and add potential scattering terms to it.

The quantum critical state arises as a result of the competition of channels 1 and 2 to form a singlet with the dot spin  $S$ . Depending on the values of the dimensionless couplings,  $J_{1,2}$ , two situations can occur:<sup>14,17</sup> (a) For  $J_1 < J_2$ , the spin of the small dot forms a Kondo singlet, with electrons on the large dot that screen the spin at an energy scale  $T^*$ . In this case, to promote a conduction electron between the left and right leads, one needs to break up the Kondo singlet and pay

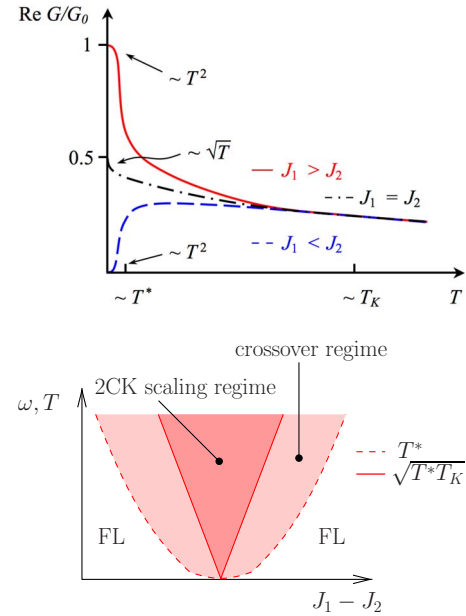


FIG. 2. (Color online) Top: Sketch of the conductance through the small dot divided by its maximum value,  $G_0$ , as a function of temperature. For  $J_1 = J_2$ , a  $\sim\sqrt{T}$  singularity emerges, while for  $J_1 \neq J_2$ , a Fermi liquid is formed at a scale  $T^*$ , and the conductance crosses over to a very small or a large value, with a characteristic Fermi-liquid scaling,  $\sim(T/T^*)^2$ . Bottom: Sketch of the “phase diagram” of the two-channel Kondo model.

an energy  $T^*$ , and therefore, transport through the small dot is suppressed at low temperatures.<sup>17,18</sup> (b) For  $J_1 > J_2$ , on the other hand, the spin of the small dot is screened by electrons in the leads. This correlated singlet state serves as a “bridge” and helps the lead electrons to propagate between the left and right sides with a small reflection probability, and is thus characterized by a conductance of the order of the quantum conductance,  $2e^2/h$ . In both cases, a Fermi-liquid state is formed below the scale  $T^*$ , which can be characterized by simple phase shifts at the Fermi energy.<sup>13</sup>

Interestingly, for  $J_1, J_2 \rightarrow J$ , the scale  $T^*$  vanishes as  $T^* \sim (J_1 - J_2)^2$ , and a non-Fermi-liquid state emerges below the Kondo scale,  $T_K \approx De^{-1/J}$ , with the cutoff  $D$  defined as  $D \equiv \min\{\delta\epsilon_s, E_{C1}, E_{C2}\}$ .<sup>14</sup> This so-called two-channel Kondo state is characterized by a conductance that is about half of the quantum conductance at very low temperatures, and has a  $\sim\sqrt{T}/T_K$  singularity for  $T \ll T_K$ .<sup>17</sup> This state is, in a sense, a quantum critical state: although it is just a single point in the parameter space, it separates two stable Fermi-liquid phases, and it influences the behavior of the double dot system over the whole regime,  $T^* < T, \omega < T_K$  for  $J_1 \approx J_2$ . However, as we shall see later, the scaling properties usually associated with the two-channel Kondo fixed point itself are restricted to a somewhat smaller energy range,  $\sqrt{T^* T_K} < T, \omega < T_K$ . The characteristic features of the temperature dependence of the dc conductance and the schematic phase diagram are sketched in Fig. 2.

The purpose of the present paper is to investigate *dynamical* transport properties of the above setup and determine how the two-channel Kondo behavior and the presence of a

quantum critical point at  $J_1=J_2$  manifest themselves in the ac conductance through the dot. For this purpose, we shall derive an expression for the ac conductance in the linear response regime that relates the conductance to the so-called composite fermions' propagator at any temperature and frequency. Making use of this simple formula, we shall evaluate the ac conductance for frequencies  $T \ll \omega$  using numerical renormalization group methods. We shall also determine the universal crossover functions that describe the non-Fermi-liquid vs Fermi-liquid crossover for  $T^* \ll T_K$ . As we will show, the ac conductance exhibits features that are qualitatively similar to the finite temperature dc conductance, sketched in Fig. 2. In addition, we shall also investigate what conclusions we can draw regarding ac properties based on the predictions of conformal field theory, and use this approach to obtain the universal scaling of the conductance in the regime  $T^* \ll \omega$ ,  $T \ll T_K$ .

The paper is organized as follows. Section II provides the details of the derivation of the ac conductance formula for the two-channel Kondo model. In Sec. III, we present some analytical considerations based on conformal field theory concerning the universal scaling properties of the linear conductance and of the eigenvalue of the so-called on-shell  $T$  matrix. Section IV comprises our numerical renormalization group results for the composite fermions' spectral function and the linear conductance in the case of channel anisotropy and in the presence of a magnetic field. Finally, our conclusions are summarized in Sec. V.

## II. KUBO FORMULA AND COMPOSITE FERMIONS

Let us start our analysis with the derivation of a simple expression for the ac conductance in terms of the so-called composite fermion operators.<sup>21</sup> For this purpose, we first couple an external voltage to the dot and introduce a time-dependent chemical potential difference between the left and right electrodes:

$$H_V \equiv V(t)Q = eV(t)(N_R - N_L), \quad (5)$$

with  $N_R$  and  $N_L$  the number of electrons in the left and right leads, respectively,

$$N_{L/R} = \sum_{\sigma} \int c_{L\sigma}^{\dagger}(\epsilon) c_{L\sigma}(\epsilon) d\epsilon.$$

The current operator can be defined as the time derivative of  $Q$ ,  $I(t) = i[H, Q(t)] = i[H_{\text{int}}, Q(t)]$ . This commutator is easily shown to give

$$I = e \frac{v_L v_R}{v_L^2 + v_R^2} J_1 (iF_1^{\dagger} \tilde{\psi}_1 + \text{H.c.}), \quad (6)$$

where  $\tilde{\psi}_1$  denotes the decoupled electron field of the leads,

$$\tilde{\psi}_1 = \frac{v_L \psi_L - v_R \psi_R}{(v_L^2 + v_R^2)^{1/2}}, \quad (7)$$

and we have introduced the so-called composite fermion operator,

$$F_{\sigma}^{\dagger} \equiv \sum_{\sigma'} \psi_{1\sigma'}^{\dagger} \tilde{\sigma}_{\sigma'\sigma} \tilde{S}. \quad (8)$$

The operator  $F^{\dagger}$  has spin 1/2 and charge 1, and it corresponds to the ‘‘universal part’’ of the electron localized on the small dot.

Close to equilibrium, the current through the dot is given by the Kubo formula

$$\langle I(t) \rangle = \int G(t-t') V(t') dt',$$

$$G(t-t') = i \langle [I(t), Q(t')] \rangle \theta(t-t'), \quad (9)$$

with  $G(t-t')$  the conductance. Differentiating with respect to time and then taking the Fourier transform, we obtain the relation

$$-i\omega G(\omega) = \mathcal{G}_{II}^R(\omega) - A, \quad (10)$$

where  $\mathcal{G}_{II}^R$  denotes the retarded current-current correlation function and  $A$  is a real constant

$$A = i \langle [Q(t'), I(t')] \rangle = \mathcal{G}_{II}^R(\omega=0). \quad (11)$$

Thus, the real and imaginary parts of the conductance are given by

$$\text{Re}\{G(\omega)\} = -\frac{1}{\omega} \text{Im}\{\mathcal{G}_{II}^R(\omega)\}, \quad (12)$$

$$\text{Im}\{G(\omega)\} = \frac{1}{\omega} (\text{Re}\{\mathcal{G}_{II}^R(\omega)\} - \text{Re}\{\mathcal{G}_{II}^R(0)\}). \quad (13)$$

In general, it is not so simple to compute the correlation function  $\mathcal{G}_{II}^R$ . In our case, however, the field  $\tilde{\psi}_1$  is completely decoupled from the spin and describes noninteracting fermions. This observation allows us to write  $\mathcal{G}_{II}^R(t)$  as

$$\begin{aligned} \mathcal{G}_{II}^R(t) = & -ie^2 \frac{v_R^2 v_L^2}{(v_R^2 + v_L^2)^2} J_1^2 \sum_{\sigma} [\mathcal{G}_{F\sigma}^R(t) \mathcal{G}_{\psi\sigma}^<(-t) + \mathcal{G}_{F\sigma}^<(t) \mathcal{G}_{\psi\sigma}^A(-t) \\ & + \mathcal{G}_{\psi\sigma}^R(t) \mathcal{G}_{F\sigma}^>(-t) + \mathcal{G}_{\psi\sigma}^>(t) \mathcal{G}_{F\sigma}^A(-t)], \end{aligned} \quad (14)$$

where  $\mathcal{G}^R$ ,  $\mathcal{G}^A$ ,  $\mathcal{G}^>$ , and  $\mathcal{G}^<$  denote the usual retarded, advanced, greater, and lesser Keldysh Green's functions. The Fourier transform of this expression simplifies considerably if one uses the fact that the field  $\tilde{\psi}_1$  is noninteracting, and therefore, the corresponding Green's functions become in the large bandwidth limit

$$\mathcal{G}_{\psi\sigma}^R(\omega) = \mathcal{G}_{\psi\sigma}^A(\omega)^* = -\frac{i}{2}, \quad \mathcal{G}_{\psi\sigma}^<(\omega) = if(\omega), \quad (15)$$

with  $f(\omega)$  the Fermi function. Taking the real and imaginary parts of the Fourier transform of Eq. (14), we finally obtain

$$\text{Re}\{G(\omega)\} = \frac{G_0}{8\omega} \sum_{\sigma} \int d\omega' \text{Im}\{t_{\sigma}(\omega')\} [f(\omega' + \omega) - f(\omega' - \omega)], \quad (16)$$

$$\text{Im}\{G(\omega)\} = \frac{G_0}{8\omega} \sum_{\sigma} \int d\omega' \text{Re}\{t_{\sigma}(\omega')\} [f(\omega' + \omega) + f(\omega' - \omega) - 2f(\omega')], \quad (17)$$

where we introduced the dimensionless eigenvalue  $t_{\sigma}(\omega)$  of the so-called on-shell  $T$  matrix,<sup>22</sup> which describes the scattering of electrons of energy  $\omega$ ,

$$t(\omega) = -J_1^2 \mathcal{G}_{F\sigma}^R(\omega), \quad (18)$$

and  $G_0$  denotes the maximum conductance through the dot,

$$G_0 = \frac{2e^2}{h} \frac{4v_L^2 v_R^2}{(v_L^2 + v_R^2)^2}. \quad (19)$$

Thus, the real part of the conductance is related to the imaginary part of  $\mathcal{G}_{F\sigma}^R$ , which is essentially the spectral function of the composite fermion,  $\varrho_{F\sigma}(\omega)$ . The latter can be determined numerically using the numerical renormalization group method. Then the real part,  $\text{Re}\{\mathcal{G}_{F\sigma}^R\}$ , can be obtained by performing a Hilbert transformation numerically, and the imaginary part of the conductance can then be calculated from  $\text{Re}\{\mathcal{G}_{F\sigma}^R\}$  by simple numerical integration. Note that Eqs. (16) and (17) provide the linear conductance through the dot for any asymmetry parameter at any temperature and any frequency. They are, thus, natural extensions of the formula given in Ref. 23, and are the analogs of the formulas obtained recently for the Anderson model.<sup>24</sup>

Equations (16) and (17) belong to the main results of our paper. We shall use these formulas to compute the ac conductance through the dot in the vicinity of the two-channel Kondo fixed point.

### III. ANALYTICAL CONSIDERATIONS

Equation (16) allows us to make numerous statements based on rather general properties of the two-channel Kondo fixed point.<sup>14</sup> From an exact theorem of Affleck and Ludwig,<sup>25</sup> e.g., we know that at the two-channel Kondo fixed point (i.e., for  $J_1=J_2$  and  $\omega, T \rightarrow 0$ ), the  $S$  matrix of the conduction electrons identically vanishes. From the relation  $S(\omega) = 1 + it(\omega)$  between the dimensionless eigenvalue of the  $S$  matrix and the  $T$  matrix, we thus obtain

$$\lim_{\omega, T \rightarrow 0} t(\omega, T) = i \quad (J_1 = J_2). \quad (20)$$

From this, it immediately follows that at the two-channel Kondo fixed point, the conductance takes half of its maximum value,

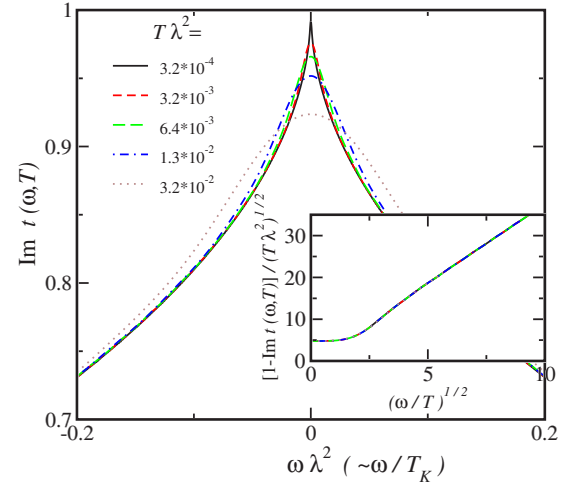


FIG. 3. (Color online) Imaginary part of the eigenvalue of the  $T$  matrix obtained by numerical integration of Eq. (22). The scale of the  $\omega$  axis is set by the amplitude of the leading irrelevant operator,  $\lambda$ . The inset illustrates how the curves corresponding to different temperatures collapse into one universal curve.

$$\lim_{\omega, T \rightarrow 0} G(\omega, T) = G_0/2 \quad (J_1 = J_2). \quad (21)$$

The results of conformal field theory<sup>25</sup> also enable us to compute the finite frequency conductance for  $J_1=J_2$  and  $\omega, T \ll T_K$ . In this limit, the  $T$  matrix is given by the expression<sup>25</sup>

$$t(\omega) = i \left\{ 1 - 3(\pi T)^{1/2} \lambda \int_0^1 du \left[ u^{-i\beta\omega/2\pi} u^{-1/2} (1-u)^{1/2} F(u) - \frac{4}{\pi} u^{-1/2} (1-u)^{-3/2} \right] \right\}, \quad (22)$$

where  $F(u) \equiv F(3/2, 3/2, 1; u)$  is the hypergeometric function, and  $\lambda$  stands for the amplitude of the leading irrelevant operator:

$$\lambda = \frac{\gamma}{\sqrt{T_K}}. \quad (23)$$

The value of the dimensionless constant  $\gamma$  depends on the precise definition of  $T_K$ . Throughout this paper, we shall define  $T_K$  as the energy at which, for  $J_1=J_2$ , the composite fermion's spectral function drops to half of its value,  $\text{Im} t(\omega=T_K) = \text{Im} t(\omega=0)/2$ . Then, comparing the numerical results of Sec. IV to the asymptotic  $\omega \gg T$  behavior of the conductance, we obtain the value  $\gamma = 0.093 \pm 0.001$ . Clearly, since the omega dependence enters  $t(\omega)$  only in the combination  $\omega/T$ , it immediately follows that  $1 - \text{Im} t(\omega, T) / (\lambda T^{1/2})$  is a universal function of  $\omega/T$  (see inset of Fig. 3).

In Fig. 3, we show the results obtained by numerically integrating Eq. (22) for a few temperatures. It is remarkable that curves corresponding to different temperatures cross each other. This feature is a direct consequence of the unusual shape of the universal curve shown in the inset of Fig. 3.

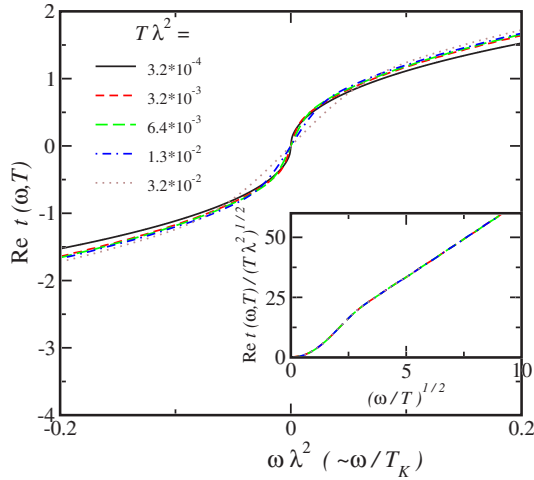


FIG. 4. (Color online) Real part of the eigenvalue  $t(\omega)$  of the  $T$  matrix predicted by conformal field theory. The inset shows the collapse to a single scaling curve (obvious from the integral definition).

Note that to construct the universal scaling curve, one needs to rescale the axes with respect to the temperature only, and the precise value of the Kondo temperature appears only through the prefactor  $\lambda$ . The fact that the only relevant energy scale is the temperature is characteristic of quantum critical points. The imaginary part of the  $T$  matrix exhibits a  $\sim\sqrt{|\omega|}$  cusp for  $T \ll \omega \ll T_K$ , and crosses over to a quadratic regime for  $\omega \ll T$ . Similar behavior is observed in the real part of  $t(\omega)$ , shown in Fig. 4. This quantity also shows a characteristic  $\sim\sqrt{\omega}$  behavior at frequencies  $T_K \gg \omega \gg T$  that crosses over to a linear regime for  $\omega \ll T$ .

Using Eqs. (22), (16), and (17), both real and imaginary parts of the conductance can be computed by numerical integration. The results are plotted in Figs. 5 and 6 for various temperatures. Even though, at first sight, the results for the conductivity look qualitatively similar to those for the  $T$  matrix, there is an important difference: integration with the

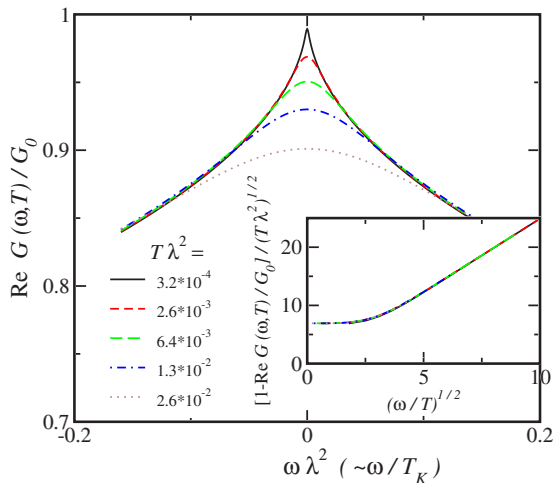


FIG. 5. (Color online) Real part of the conductance computed from Eqs. (22), (16), and (17). The inset shows the universal collapse.

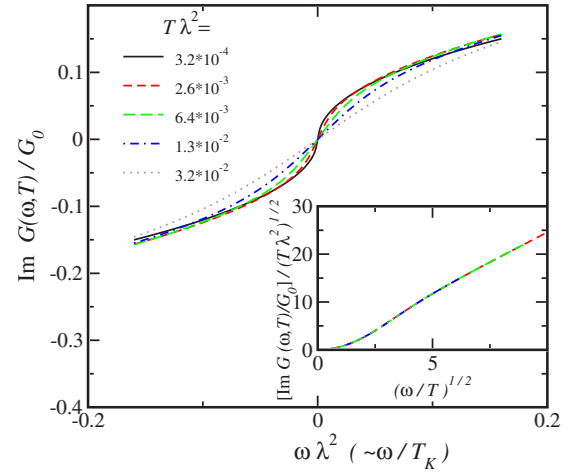


FIG. 6. (Color online) Imaginary part of the conductance from Eqs. (22), (16), and (17). The inset shows the universal scaling curve.

Fermi functions apparently eliminated the aforementioned crossing of the curves. Similar scaling curves have been computed using conformal field theory results for the differential conductance of two-channel Kondo scatterers in point contacts.<sup>26</sup>

In the limit  $T_K \gg \omega \gg T$ , the conformal field theory also predicts that the ac conductance scales as

$$\begin{aligned} \text{Re } G(\omega) &\approx \frac{G_0}{2} \left( 1 - \alpha \sqrt{\frac{\omega}{T_K}} \right), \\ \text{Im } G(\omega) &\approx \frac{G_0}{2} \alpha \text{sign}(\omega) \sqrt{\frac{|\omega|}{T_K}}, \end{aligned} \quad (24)$$

with  $\alpha = 2.53 \pm 0.06$  a universal constant of order unity. The fact that the coefficients in the two equations above are both equal to  $\alpha$  follows from the observation that  $G(\omega)$  is analytical in the upper half-plane.

For  $J_1 \neq J_2$ , a new Fermi-liquid scale,  $T^*$  (mentioned earlier), emerges, but one can still make many statements based on the fact that the leading relevant and irrelevant operators have scaling dimensions  $y_+ = 1/2$  and  $y_- = -1/2$ , respectively.<sup>14</sup> As a consequence, in the vicinity of the two-channel Kondo fixed point ( $T^* \ll T_K$ ), the conductance becomes a function of the form

$$G(\omega, T) = G\left(\frac{\omega}{T_K}, \frac{T}{T_K}, \frac{T^*}{T_K}\right), \quad (25)$$

with the Fermi-liquid scale  $T^*$  approximately given by

$$T^* \approx T_K K_R^2 \sim (J_1 - J_2)^2, \quad (26)$$

where we introduced the renormalized anisotropy parameter  $K_R$  as

$$K_R \equiv \frac{4(J_1 - J_2)}{(J_1 + J_2)^2}. \quad (27)$$

Throughout this paper, we shall define  $T^*$  as the energy scale at which  $\text{Im } t(\omega = T^*) = 1.5$  in the channel of larger coupling.

Note that the parameter  $K_R$  can be considerably larger than the naive estimate,  $(J_1 - J_2)/(J_1 + J_2)$ , due to the renormalization of the couplings  $J_1$  and  $J_2$  in the high energy regime,  $D > \omega > T_K$ . In the limit of  $T^*$ ,  $\omega \ll T_K$  and  $T \rightarrow 0$ , the conductance  $G(\omega, T)$  becomes a universal function of  $\omega/T^*$ ,

$$G_{\{\omega, T^*\} \ll T_K}(\omega, T=0) = G_0 F_{\pm}(\omega/T^*). \quad (28)$$

The signs  $\pm$  refer to the cases  $J_1 > J_2$  and  $J_1 < J_2$ , respectively, and the scaling functions  $F_{\pm}(y)$  have the properties

$$\text{Re } F_{\pm}\left(\frac{\omega}{T^*}\right) \approx \begin{cases} a_{\pm} + b_{\pm} \left(\frac{\omega}{T^*}\right)^2, & \omega \ll T^* \\ \frac{1}{2} \pm c \left(\frac{T^*}{\omega}\right)^{1/2}, & \omega \gg T^*. \end{cases} \quad (29)$$

In other words, for  $\omega \ll T^*$ , the conductance through the dot is Fermi-liquid-like, and  $\text{Re } G$  shows a  $\sim(\omega/T^*)^2$  behavior, while for  $T_K \gg \omega \gg T^*$ , the real part of the conductance scales to its two-channel Kondo value with a small but increasing correction,  $\sim\sqrt{T^*}/\omega$ . The latter behavior breaks down once the amplitude of the leading irrelevant operator,  $\sim\sqrt{\omega/T_K}$ , reaches that of the anisotropy operator,  $\sim\sqrt{T^*}/\omega$ , i.e., at frequencies in the range  $\omega \approx \sqrt{T_K T^*}$ . The constants  $a_{\pm}$ ,  $b_{\pm}$ , and  $c$  above are numbers of order unity that depend somewhat on electron-hole symmetry breaking, but close to electron-hole symmetry,  $a_+ \approx 1$  and  $a_- \approx 0$ . Note that the precise value of the constants  $b_{\pm}$  and  $c$  depends also on the definition of the scale  $T^*$ .

The imaginary part of  $F_{\pm}(y)$  has somewhat different properties and behaves as

$$\text{Im } F_{\pm}\left(\frac{\omega}{T^*}\right) \approx \begin{cases} d_{\pm} \frac{\omega}{T^*} & \text{for } \omega \ll T^* \\ \pm e \left(\frac{T^*}{\omega}\right)^{1/2} & \text{for } \omega \gg T^*. \end{cases} \quad (30)$$

In other words, the imaginary part of  $G$  must show a bump of size  $\sim G_0$  at frequencies  $\omega \sim T^*$ . These expectations shall, indeed, be met by our numerical results.

Similar to channel asymmetry, an external magnetic field also suppresses the non-Fermi-liquid behavior<sup>14</sup> and introduces a new Fermi-liquid scale,

$$T_B \equiv \frac{B^2}{T_K}. \quad (31)$$

However, the magnetic field does not result in such a dramatic change in the conductance as the channel-symmetry breaking: while at  $\omega=0$  the conductance exhibits a *jump* as a function of the channel anisotropy, it changes continuously as a function of the magnetic field and shows only a cusp,<sup>20,27</sup>

$$G(B)_{J_1=J_2} \approx \frac{G_0}{2} \left( 1 - \beta \frac{|B|}{T_K} \ln \left( \frac{T_K}{|B|} \right) \right), \quad (32)$$

as it obviously follows from the singular behavior of the conduction electron phase shifts at the Fermi energy.<sup>27,28</sup> As we shall see later, the ac conductance displays much more interesting features in a finite magnetic field.

## IV. NUMERICAL RESULTS

In this section, we shall use the numerical renormalization group (NRG) method<sup>29</sup> to compute the eigenvalue of the  $T$  matrix, and from that, the ac conductance. Although Eqs. (16) and (17) hold at any temperature, finite temperature calculations are extremely delicate close to a non-Fermi-liquid state. Therefore, we shall present numerical results only for  $T=0$  here. Nevertheless, according to the basic principles of scaling, a finite frequency  $\omega$  plays a role rather similar to that of a finite temperature, and therefore, the  $T=0$  ac conductance,  $G(\omega, T=0)$ , behaves rather similarly to the dc conductance at a finite temperature  $T$ ,  $G(\omega=0, T)$ .

To perform accurate calculations, we assumed an electron-hole symmetrical conduction band and strongly exploited the symmetries of the Hamiltonian. The numerical results presented here have been obtained using a different “flexible” NRG code, which made it possible to use together with an arbitrary number of SU(2) spin and charge symmetries.<sup>30</sup> The generators of these symmetries can be found in the Appendix.

In particular, in the absence of an external magnetic field, we used a symmetry  $\text{SU}_{c_1}(2) \otimes \text{SU}_{c_2}(2) \otimes \text{SU}_s(2)$ , with  $\text{SU}_{c_1}(2)$  and  $\text{SU}_{c_2}(2)$  the charge SU(2) symmetries in channels 1 and 2, respectively,<sup>31</sup> and  $\text{SU}_s(2)$  the spin SU(2) symmetry. The advantage of this symmetry is that it is not violated even for  $J_1 \neq J_2$ , and it breaks down only to  $\text{SU}_{c_1}(2) \otimes \text{SU}_{c_2}(2) \otimes \text{U}_s(1)$  in the presence of a magnetic field. For the channel anisotropic cases, we have retained a maximum of 750 multiplets during the NRG calculations, whereas 850 multiplets were kept in the presence of a magnetic field. All calculations were carried out with a discretization parameter  $\Lambda=2$ . To compute the ac conductance, we have determined the composite fermion’s spectral function, which, apart from an overall normalization factor, is equal to  $\text{Im } t(\omega)$ . This normalization factor can be easily fixed for  $J_1=J_2$  using the condition of Eq. (20). This procedure is much more accurate than estimating the normalization factor from the bare couplings, since the latter procedure suffers from the NRG discretization problem as well as from the loss of spectral weight at high energies, leading generally to a few percent error in the amplitude.

### A. Channel-symmetry breaking

First, we investigated numerically how the non-Fermi-liquid structure appears in the ac conductance through the double dot and how channel anisotropy destroys this non-Fermi-liquid behavior. Some typical results are shown in Fig. 7: for  $J_1=J_2$ , we recover the two-channel Kondo result,  $\text{Im } t(\omega \rightarrow 0) = 1$ , and the deviation from the fixed point value scales as  $\sim\sqrt{\omega/T_K}$ , in agreement with Eq. (24).

For  $J_1 \neq J_2$ , the new crossover scale  $T^*$  appears, below which  $\text{Im } t(\omega)$  crosses over from the two-channel Kondo value  $\text{Im } t(\omega)=1$  to  $\text{Im } t(\omega)=2$  for  $J_1 > J_2$  or to  $\text{Im } t(\omega)=0$  for  $J_1 < J_2$  in the electron-hole symmetrical situation studied numerically. In the limit  $T^* \ll T_K$ , this crossover is described

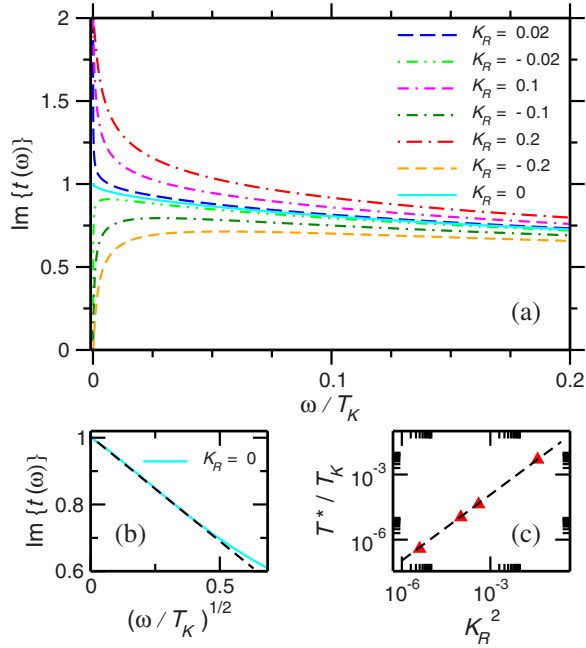


FIG. 7. (Color online) (a) Imaginary part of the eigenvalue of the on-shell  $T$  matrix, as function of  $\omega/T_K$ , for several different values of the anisotropy parameter,  $K_R=4(J_1-J_2)/(J_1+J_2)^2$ . In all cases,  $J_1+J_2=0.2$ . Curves with  $J_1>J_2$  or  $J_1<J_2$  scale to  $\text{Im } t(0)=2$  or  $\text{Im } t(0)=0$ , respectively. The critical curve corresponding to  $J_1=J_2$  separates these two sets of curves. (b)  $\text{Im } t(\omega)$  for  $J_1=J_2$  as a function of  $\sqrt{\omega/T_K}$ . The dashed line is a guide for the eye. (c)  $T^*$  as a function of  $K_R^2$ .

by universal crossover functions, similar to Eq. (29). We determined these scaling functions numerically and displayed them in Fig. 8. (The black curves were obtained by taking an extremely small value of  $T^*$  and chopping off the parts near  $\omega \sim T_K$ .) The Fermi-liquid scale  $T^*$  extracted from  $t(\omega)$  is

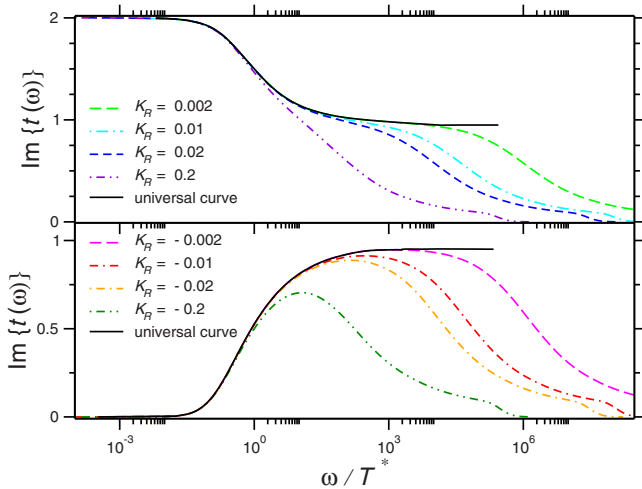


FIG. 8. (Color online) Imaginary part of the on-shell  $T$  matrix in the presence of channel anisotropy as a function of  $\omega/T^*$ . The upper part corresponds to  $J_1>J_2$ , while the lower part to  $J_1<J_2$ . In both cases, for  $T^*, \omega \ll T_K$ , the curves follow the universal crossover function, corresponding to a  $(\omega/T^*)^2$ -like scaling at low frequencies and a  $1 \pm c(T^*/\omega)^{1/2}$  behavior at large frequencies.

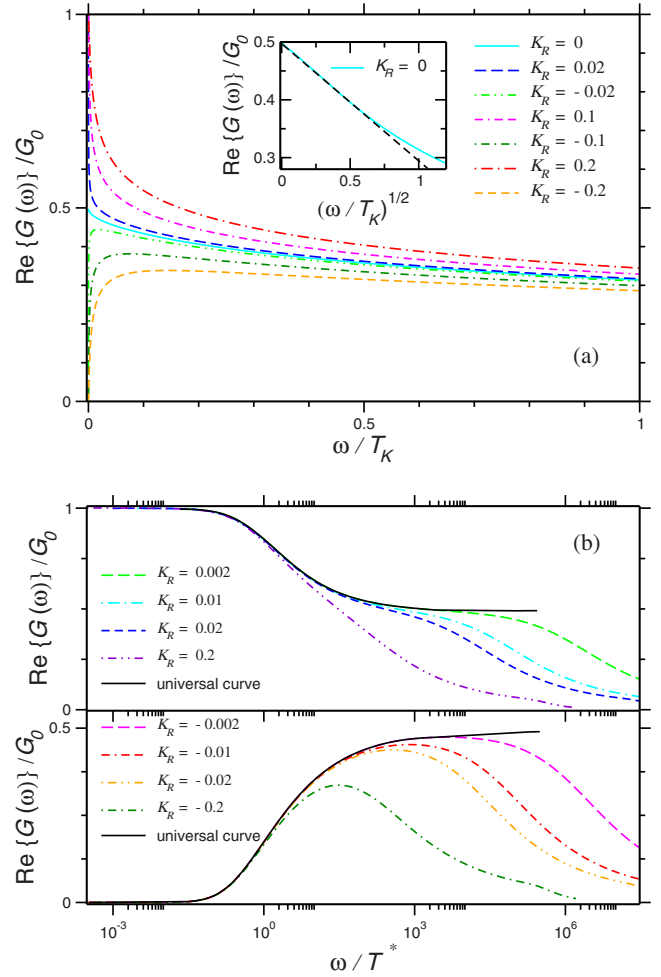


FIG. 9. (Color online) (a) ac conductance as a function of  $\omega/T_K$ . For  $J_1>J_2$  and  $J_1<J_2$ , the curves scale as  $\text{Re } G \rightarrow G_0$  and  $\text{Re } G \rightarrow 0$ , respectively. Inset: ac conductance for  $J_1=J_2$  as a function of  $\sqrt{\omega/T_K}$ . (b) ac conductance for positive (upper part) and negative (lower part) channel anisotropy parameters as a function of  $\omega/T^*$ . For  $\omega, T^* \ll T_K$ , the curves follow the universal crossover curves.

shown in Fig. 7(c), and is in excellent agreement with the analytical expression of Eq. (26).

According to Eq. (16), the real part of the conductance can be computed from  $\text{Im } t(\omega)$  through a simple integration. The resulting conductance curves are shown in Fig. 9. The behavior of  $\text{Re } G(\omega)$  is strikingly similar to that of  $\text{Im } t$ : it also exhibits a  $\sim \sqrt{\omega}$  singularity for  $J_1=J_2$  and crosses over from a value  $G=G_0/2$  to  $G=G_0$  or to  $G=0$  at the scale  $T^*$  following the universal crossover functions,  $F_{\pm}(\omega/T^*)$ . We remark here that there seems to be no other reliable way than NRG to determine these universal crossover functions, which connect two separate strong coupling fixed points, the non-Fermi-liquid fixed point and the Fermi-liquid fixed point. These universal crossover functions constitute some of the central results of this work.

Performing a Hilbert transform, we also determined numerically the real part of the  $T$  matrix,  $\text{Re } t(\omega)$ , and from that, the imaginary part of the conductance. These results are shown in Fig. 10. It is quite remarkable that, although the

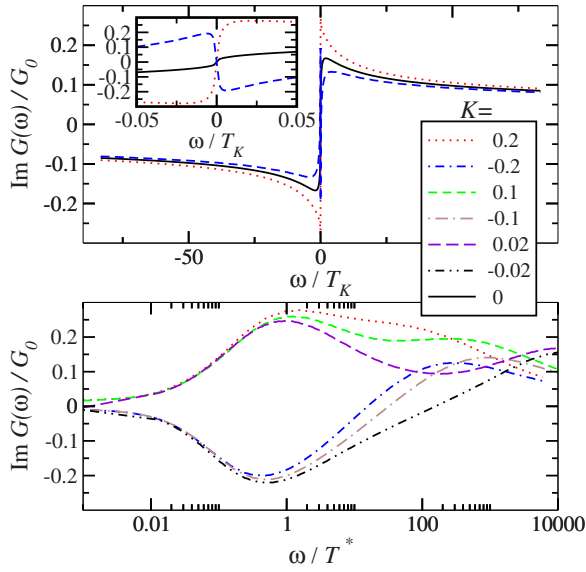


FIG. 10. (Color online) Imaginary part of the ac conductance as a function of  $\omega/T_K$ . Lower panel: Same as that of the upper panel but as a function of  $\omega/T^*$ .

scaling is not perfect because of insufficient accuracy of the Hilbert transform and the various integrations, clearly, the *amplitude* of the low temperature peak at  $\omega \sim T^*$  does not change as  $T^*$  goes to 0. (Note that  $T^*$  varies over 2 orders of magnitudes.) This behavior is, indeed, expected based on Eq. (30). The numerical results confirm that for  $J_1 > J_2$  and  $J_1 < J_2$ , the coefficients  $d_{\pm}$  have different signs,  $d_+ > 0$  and  $d_- < 0$ , and that  $\text{Im } G(\omega)$  has a *double peak structure*: it has one peak at  $\omega \sim T_K$  corresponding to the crossover to the two-channel Kondo fixed point, and also another peak at  $\omega \sim T^*$  related to the non-Fermi-liquid–Fermi-liquid crossover.

It is interesting to observe from Figs. 8–10 that the range of two-channel Kondo scaling does *not* reach from  $T_K$  down to the crossover scale  $T^*$ , but rather it stops at a much higher energy scale,  $\sim \sqrt{T^* T_K}$ , where corrections from the leading relevant operators start to dominate over the leading irrelevant operator of the two-channel Kondo fixed point.

### B. Effects of magnetic field

We also performed calculations for  $J_1 = J_2$  in the presence of a local magnetic field  $B$ . As mentioned earlier, a small local magnetic field destroys the non-Fermi-liquid state and drives the system to a trivial, Fermi-liquid fixed point below a scale  $T_B = B^2/T_K \ll T_K$ .<sup>28</sup>

Some typical results are shown in Fig. 11. At large magnetic fields,  $B > T_K$ , the Kondo resonance is clearly split below the Zeeman field, and  $\text{Re } G(\omega)$  exhibits a dip for  $|\omega| < B$ . The width of this dip gradually decreases as one decreases the size of the field  $B$ , and its depth becomes smaller and smaller. However, it is not clear from the numerics if there is a critical field value  $B_C$  below which the dip actually disappears, as is the case, e.g., for the single-channel Kondo model. In fact, the numerical results seem to show just the opposite, i.e., that  $\text{Re } G(\omega)$  remains a *nonmonotonous* func-

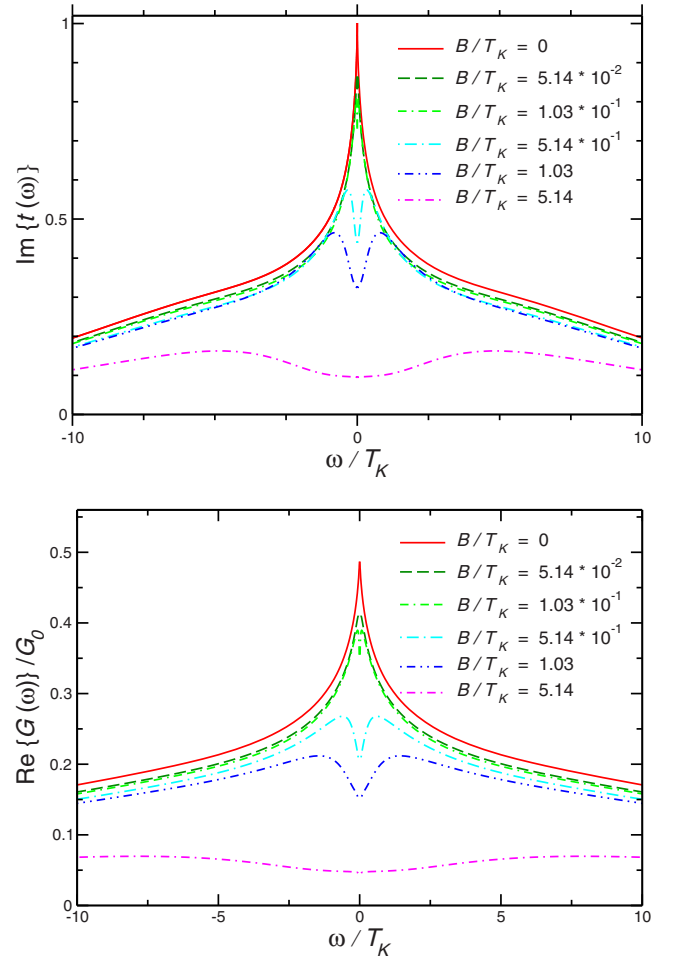


FIG. 11. (Color online) Top: Imaginary part of the on-shell  $T$  matrix in the presence of a magnetic field and no channel asymmetry, as a function of  $\omega/T_K$ . Lower curves correspond to higher magnetic fields. Bottom: ac conductance in the presence of a magnetic field and no channel asymmetry, as a function of  $\omega/T_K$ . Lower curves correspond to higher magnetic field values.

tion in *any* finite magnetic field, and only the height and width of the dip at  $\omega \sim T_B$  get smaller and smaller for smaller magnetic fields, while the dip itself is always present. This would, indeed, naturally follow from a simple scaling argument: for  $B < T_K$ , a magnetic energy scale is generated,  $T_B = B^2/T_K$ , and at this energy, the real part of the conductance is expected to be  $\text{Re } G(\omega \approx T_B) \approx G_0[1/2 - \alpha|B|/T_K]$ . On the other hand, from Bethe Ansatz<sup>32</sup> we know the exact phase shifts, and from that, it immediately follows that the dc conductance is given by  $G(\omega=0) \approx G_0(1/2) - (C|B|/T_K) \log(T_K/|B|)$  at  $T=0$ , with  $C$  a constant of the order of unity.<sup>27</sup> This observation suggests that in any finite magnetic field,  $G(\omega)$  displays a dip, which has a width  $\Delta\omega \sim T_B$  and height  $\Delta G \sim (|B|/T_K) \log(T_K/|B|)$ . Similar behavior is expected as a function of temperature, too.

It is not clear either if  $G(\omega)$  becomes a universal function of  $\omega/T_B$ . In fact, it has been shown in a special, very anisotropic limit that no such universal function exists for the nonlinear dc conductance.<sup>33</sup> We can argue that the same

probably holds for the linear ac conductance, although we do not have a rigorous proof.

Unfortunately, from a numerical point of view, the calculations in a magnetic field turned out to be extremely difficult: first of all, for the positive and negative frequency parts of the spectral function, one loses somewhat different amounts of spectral weight. This effect turns out to be extremely large in the two-channel Kondo case, probably as a consequence of the extreme sensitivity of the non-Fermi-liquid fixed point to the magnetic field. Therefore, for a given spin direction, one needs to *match* these positive- and negative-frequency parts at the origin. Although this is a standard procedure followed by most groups, this leads to a large uncertainty in case of the two-channel Kondo model. In fact, despite the extensive symmetries used, we were not able to obtain data of sufficient accuracy in the most interesting regime,  $\omega \ll T_B = B^2/T_K \ll T_K$ , even using Hofstetter's density matrix NRG method.<sup>34</sup> Therefore, we were not able to investigate the issue of universal crossover functions for  $J_1 = J_2$  and  $T_B = B^2/T_K \ll T_K$ . We, therefore, consider these numerical results only as indicative but not decisive.

We also need to recall the well-known fact that NRG produces an artificial broadening proportional to  $\omega$  of the peaks occurring at finite frequencies. Thus, the correct shape of these split peaks is presumably significantly sharper than that shown by the NRG results.

## V. CONCLUSIONS

In this paper, we have studied the ac transport properties of a double dot device realized recently by Potok *et al.* to reach the two-channel Kondo fixed point. First, we derived an analytical expression for the linear conductance in the regime where charge fluctuations are small and the system can be described by a Kondo Hamiltonian. Our formula relates the ac conductance to the eigenvalue  $t(\omega)$  of the dimensionless on-shell  $T$  matrix, and is valid at any temperature and for any frequency. Our expression is the analog of the formula obtained recently by Sindel *et al.* for the Anderson model,<sup>24</sup> and it carries over to most Kondo-type Hamiltonians.

The general properties of the two-channel Kondo fixed point, known from conformal field theory, allowed us to make many quantitative and qualitative predictions for the ac conductance,  $G(\omega)$ : for equal couplings to the two channels,  $G(\omega)$  shows a  $\sqrt{\omega/T_K}$  singularity at the two-channel Kondo fixed point. Using the results of conformal field theory,<sup>25</sup> we were able to compute the real and imaginary parts of the function  $G(\omega, T)$  and determine the corresponding scaling functions for both real and imaginary parts of the conductance through the dot in the universal regime,  $\omega, T \ll T_K$  and  $J_1 = J_2$ . The generic properties of the ac conductance in this regime are summarized in Fig. 12.

Conformal field theory also gave us a way to predict the basic properties of  $\text{Re } G(\omega)$  and  $\text{Im } G(\omega)$  at  $T=0$  in the presence of channel-symmetry breaking (see Fig. 13). For  $J_1 \neq J_2$ ,  $\text{Re } G(\omega)$  crosses over to a much smaller or a much larger value (depending on the sign of asymmetry) at the Fermi-liquid scale  $T^*$ , below which it becomes an analytical

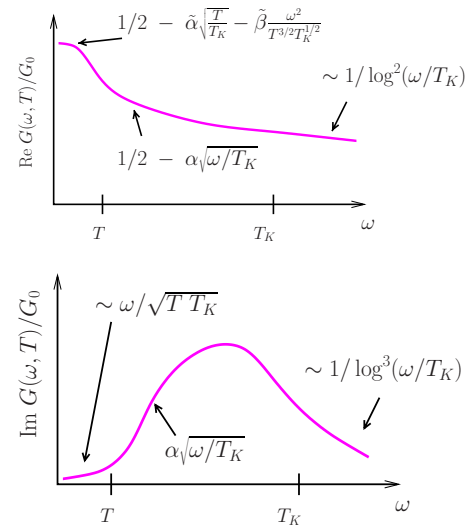


FIG. 12. (Color online) Sketch of the real and imaginary parts of the ac conductance for  $J_1 = J_2$  and  $\omega, T \ll T_K$ .

function of  $\omega$ . This crossover at  $\omega \sim T^*$  is described by universal crossover functions that we have determined numerically. The asymptotic properties of the real and imaginary parts of the conductance are dictated by conformal field theory [see Eqs. (29) and (30)]. It is quite remarkable that  $\text{Im } G(\omega)$  shows a double peak structure at frequencies  $\omega \sim T^*$  and  $\omega \sim T_K$ . Both peaks are of amplitude  $\sim G_0$ , but the

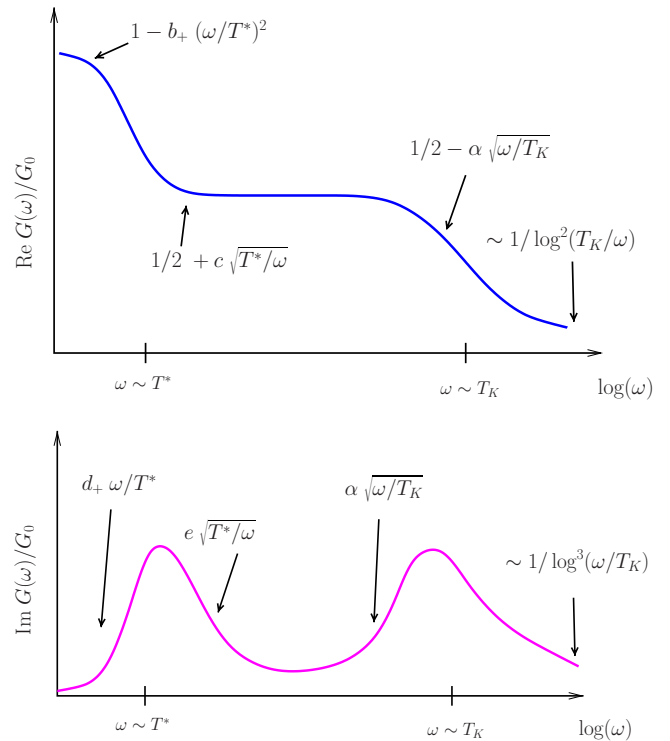


FIG. 13. (Color online) Sketch of the real and imaginary parts of the  $T=0$  ac conductance for  $J_1 > J_2$ . The various powers shown in the picture follow from conformal field theory. The high frequency behavior is a result of perturbation theory. We assumed electron-hole symmetry.

sign of the peak at  $\omega \sim T^*$  changes with the sign of  $J_1 - J_2$ .

One of the important conclusions that one could draw from the analysis of  $G(\omega)$  was that the two-channel Kondo regime is, in a sense, restricted to the regime  $\sqrt{T_K T^*} < T$ ,  $\omega < T_K$ : Although it is true that the entire regime,  $T^* < T$ ,  $\omega < T_K$  is governed by the two-channel Kondo fixed point, for  $T$ ,  $\omega < \sqrt{T_K T^*}$  the leading relevant operator is more important than the leading irrelevant operator, and therefore, the scaling curves characteristic to the two-channel Kondo fixed point itself cannot be seen in this regime. This refines somewhat the phase diagram of the two-channel Kondo model, as already indicated in Fig. 2. The two-channel Kondo scaling regime is, thus, limited by a boundary  $\sim |J_1 - J_2|$ .

We have also investigated the effects of a small Zeeman field on the ac conductance. For  $B > T_K$ , the ac conductance exhibits a dip whose width is just  $B$ . Numerically, we find that, apparently, this dip survives for any small magnetic field,  $B < T_K$ . This would, indeed, be in agreement with a simple scaling argument we presented that also predicts a similar behavior as a function of temperature. In other words, at the two-channel Kondo fixed point, the Kondo resonance appears to be split at any magnetic field. Unfortunately, while our numerics seems to support this picture, it is not accurate enough in the regime  $B \ll T_K$  to give a decisive answer. We remark that the logarithmic magnetic field dependence of the phase shift would also probably imply that universal scaling (i.e.,  $T/T_B$  scaling and the disappearance of the scale  $T_K$  for  $T, T_B \ll T_K$ ) should be destroyed by logarithmic corrections in the presence of a magnetic field.

#### ACKNOWLEDGMENTS

We would like to thank F. Anders, A. Schiller, and L. Udvardi for helpful discussions. This research has been supported by Hungarian OTKA Grants Nos. NF061726, T046267, T046303, and D048665, by the DFG Center for Functional Nanostructures (CFN), and by Sonderforschungsbereich 631. G.Z. acknowledges the hospitality of the CAS, Oslo. L.B. acknowledges the financial support from the Bolyai Foundation.

TABLE I. Generators of the symmetries used for the two-channel Kondo model computations. Sites along the Wilson chain are labeled by  $n$ , whereas  $\alpha$  and  $\mu, \nu$  are the channel and spin indices, respectively.

Symmetry group	Generators
$SU_{C\alpha}(2)$	$Q_{\alpha}^{\dagger} = \sum_{n=0}^{\infty} (-1)^n f_{n,\alpha,\uparrow}^{\dagger} f_{n,\alpha,\downarrow}$ $Q_{\alpha}^z = 1/2 \sum_{n=0}^{\infty} \sum_{\mu} (f_{n,\alpha,\mu}^{\dagger} f_{n,\alpha,\mu} - 1)$ $Q_{\alpha}^{-} = Q_{\alpha}^{\dagger}$
$SU_s(2)$	$\vec{J} = \vec{S} + 1/2 \sum_{n=0}^{\infty} \sum_{\alpha,\mu,\nu} f_{n,\alpha,\mu}^{\dagger} \vec{\sigma}_{\mu\nu} f_{n,\alpha,\nu}$
$U_s(1)$	$J^z = S^z + 1/2 \sum_{n=0}^{\infty} \sum_{\alpha,\mu,\nu} f_{n,\alpha,\mu}^{\dagger} \sigma_{\mu\nu}^z f_{n,\alpha,\nu}$

#### APPENDIX: SYMMETRY GENERATORS

We rewrite the Hamiltonian in a form appropriate for NRG calculations as

$$H = H_{\text{int}} + \sum_n \sum_{\alpha,\mu,\nu} t_n (f_{n,\alpha,\mu}^{\dagger} f_{n+1,\alpha,\mu} + \text{H.c.}),$$

$$H_{\text{int}} = \vec{S} \sum_{\alpha,\mu,\nu} \frac{\vec{J}_{\alpha}}{2} f_{0,\alpha,\mu}^{\dagger} \vec{\sigma}_{\mu\nu} f_{0,\alpha,\mu}. \quad (\text{A1})$$

Here,  $\vec{S}$  is the impurity spin operator, the  $f_0$ 's are anticommuting operators at the impurity site, and  $\alpha$  and  $\mu, \nu$  stand for the channel and spin indices, respectively. The  $J_{\alpha}$ 's are the couplings, and  $\vec{\sigma}$  is the vector triad of Pauli matrices. The second part of the Hamiltonian is the so-called Wilson chain: it describes electrons hopping along a semi-infinite chain with a hopping  $t_n \sim \Lambda^{-n/2}$ , and accounts for the dynamics of those electrons that couple to the impurity.

The Hamiltonian above is invariant under the symmetry  $SU_{c1}(2) \otimes SU_{c2}(2) \otimes SU_s(2)$ , with the symmetry generators listed in Table I. The first two symmetries are related to electron-hole symmetry, while the third one corresponds to the conservation of spin. In the presence of a magnetic field, the symmetry of the system breaks down to  $SU_{c1}(2) \otimes SU_{c2}(2) \otimes U_s(1)$ , the symmetry  $U_s(1)$  corresponding to the conservation of the  $z$  component of the spin (see Table I).

<sup>1</sup>For a review, see e.g., L. I. Glazman and M. Pustilnik, in *Nanophysics: Coherence and Transport*, edited by H. Bouchiat *et al.* (Elsevier, New York, 2005), pp. 427–478.

<sup>2</sup>For reviews, see, e.g., G. Schön and A. D. Zaikin, *Phys. Rep.* **198**, 237 (1990); or G.-L. Ingold and Y. V. Nazarov, in *Single Charge Tunneling*, edited by H. Grabert and M. Devoret, NATO Advanced Studies Institute, Series B: Physics (Plenum, New York, 1992), Vol. 294, pp. 21–107.

<sup>3</sup>R. Wilkins, E. Ben-Jacob, and R. C. Jaklevic, *Phys. Rev. Lett.* **63**, 801 (1989).

<sup>4</sup>D. Goldhaber-Gordon, H. Shtrikman, D. Mahalu, D. Abusch-Magder, U. Meirav, and M. A. Kastner, *Nature (London)* **391**, 156 (1998); S. M. Cronenwett, T. H. Oosterkamp, and L. P. Kouwenhoven, *Science* **281**, 540 (1998); J. Schmid, J. Weis, K.

Eberl, and K. von Klitzing, *Physica B* **256-258**, 182 (1998).

<sup>5</sup>See, e.g., L. Borda, G. Zaránd, W. Hofstetter, B. I. Halperin, and J. von Delft, *Phys. Rev. Lett.* **90**, 026602 (2003).

<sup>6</sup>D. Loss and D. P. DiVincenzo, *Phys. Rev. A* **57**, 120 (1998).

<sup>7</sup>W. Hofstetter and H. Schoeller, *Phys. Rev. Lett.* **88**, 016803 (2001); M. Vojta, R. Bulla, and W. Hofstetter, *Phys. Rev. B* **65**, 140405(R) (2002).

<sup>8</sup>A. Kogan, G. Granger, M. A. Kastner, D. Goldhaber-Gordon, and H. Shtrikman, *Phys. Rev. B* **67**, 113309 (2003).

<sup>9</sup>S. Sasaki, S. De Franceschi, J. M. Elzerman, W. G. van der Wiel, M. Eto, S. Tarucha, and L. P. Kouwenhoven, *Nature (London)* **405**, 764 (2000); J. Schmid, J. Weis, K. Eberl, and K. v. Klitzing, *Phys. Rev. Lett.* **84**, 5824 (2000).

<sup>10</sup>M. Pustilnik, L. I. Glazman, and W. Hofstetter, *Phys. Rev. B* **68**,

- 161303(R) (2003); W. Hofstetter and G. Zaránd, *ibid.* **69**, 235301 (2004).
- <sup>11</sup>K. Le Hur, Phys. Rev. Lett. **92**, 196804 (2004).
- <sup>12</sup>L. Borda, G. Zaránd, and P. Simon, Phys. Rev. B **72**, 155311 (2005); M.-R. Li, K. Le Hur, and W. Hofstetter, Phys. Rev. Lett. **95**, 086406 (2005).
- <sup>13</sup>Ph. Nozières, J. Low Temp. Phys. **17**, 31 (1974).
- <sup>14</sup>D. L. Cox and A. Zawadowski, Adv. Phys. **47**, 599 (1998).
- <sup>15</sup>B. A. Jones, C. M. Varma, and J. W. Wilkins, Phys. Rev. Lett. **61**, 125 (1988); B. A. Jones and C. M. Varma, Phys. Rev. B **40**, 324 (1989); J. B. Silva, W. L. C. Lima, W. C. Oliveira, J. L. N. Mello, L. N. Oliveira, and J. W. Wilkins, Phys. Rev. Lett. **76**, 275 (1996).
- <sup>16</sup>K. A. Matveev, Zh. Eksp. Teor. Fiz. **98**, 1598 (1990) [Sov. Phys. JETP **72**, 892 (1991)]; Phys. Rev. B **51**, 1743 (1995).
- <sup>17</sup>Y. Oreg and D. Goldhaber-Gordon, Phys. Rev. Lett. **90**, 136602 (2003).
- <sup>18</sup>R. M. Potok, I. G. Rau, H. Shtrikman, Y. Oreg, and D. Goldhaber-Gordon, Nature (London) **446**, 167 (2007).
- <sup>19</sup>G. Zaránd, C.-H. Chung, P. Simon, and M. Vojta, Phys. Rev. Lett. **97**, 166802 (2006).
- <sup>20</sup>F. B. Anders, E. Lebanon, and A. Schiller, Phys. Rev. B **70**, 201306(R) (2004); F. B. Anders, *ibid.* **71**, 121101(R) (2005).
- <sup>21</sup>T. A. Costi, Phys. Rev. Lett. **85**, 1504 (2000).
- <sup>22</sup>L. Borda, L. Fritz, N. Andrei, and G. Zaránd, Phys. Rev. B **75**, 235112 (2007).
- <sup>23</sup>M. Pustilnik and L. I. Glazman, Phys. Rev. B **64**, 045328 (2001).
- <sup>24</sup>M. Sindel, W. Hofstetter, J. von Delft, and M. Kindermann, Phys. Rev. Lett. **94**, 196602 (2005).
- <sup>25</sup>I. Affleck and A. W. W. Ludwig, Phys. Rev. B **48**, 7297 (1993).
- <sup>26</sup>J. von Delft, A. W. W. Ludwig, and V. Ambegaokar, Ann. Phys. **273**, 175 (1998).
- <sup>27</sup>M. Pustilnik, L. Borda, L. I. Glazman, and J. von Delft, Phys. Rev. B **69**, 115316 (2004).
- <sup>28</sup>I. Affleck, A. W. W. Ludwig, H.-B. Pang, and D. L. Cox, Phys. Rev. B **45**, 7918 (1992).
- <sup>29</sup>K. G. Wilson, Rev. Mod. Phys. **47**, 773 (1975); for a recent review, see R. Bulla, T. A. Costi, and T. Pruschke, arXiv:cond-mat/0701105 (unpublished).
- <sup>30</sup>A. I. Tóth, L. Borda, and G. Zaránd (unpublished).
- <sup>31</sup>B. A. Jones, C. M. Varma, and J. W. Wilkins, Phys. Rev. Lett. **61**, 125 (1988).
- <sup>32</sup>N. Andrei and C. Destri, Phys. Rev. Lett. **52**, 364 (1984).
- <sup>33</sup>A. Schiller and S. Hershfield, Phys. Rev. B **51**, 12896 (1995).
- <sup>34</sup>W. Hofstetter, Phys. Rev. Lett. **85**, 1508 (2000).